Use of the two-ion hybrid as an impurity diagnostic

Francis F. Chen,[a] G. Dimonte, T. Christensen, G. R. Neil, and T. E. Romesser
Energy Development Group, TRW, Redondo Beach, California 90278

(Received 10 May 1985; accepted 2 January 1986)

In a plasma containing more than one ion species, the frequencies of the ion–ion hybrid resonances can be a sensitive measure of the densities of the minor species, but only if the frequency shifts caused by electron motions are small, as experimental observations suggest. By calculating the eigenfrequencies for ion–ion hybrid waves taking into account collisions, Landau damping, electron inertia, electromagnetic effects, and density gradients, it is found that the frequency shifts are not negligible unless $k_\parallel$ is extremely small. Treatment of the sheath boundary conditions at the ends of a plasma column shows that the effective value of $k_\parallel$ can indeed be sufficiently small, and that the uncorrected resonance frequency is surprisingly accurate over a wide parameter range. Data from an Ar–Xe discharge demonstrate the usefulness of this technique for measuring impurity concentrations.

I. INTRODUCTION

The Buchsbaum two-ion hybrid resonance frequency[1] ω_r given by

$$\omega_r^2 = \Omega_1\Omega_2[(\alpha_1\Omega_2 + \alpha_2\Omega_1)/(\alpha_1\Omega_1 + \alpha_2\Omega_2)]\,, \qquad (1)$$

where $\alpha_{1,2}$ and $\Omega_{1,2}$ are the fractional charge densities and cyclotron frequencies of species 1 and 2, respectively, can in principle be used to measure impurity concentrations in a plasma. For instance, the nonhydrogenic contaminants in a diverted fusion plasma, the molecular ion (H_2^+) fraction in a hydrogen discharge, or the fraction of doubly charged ions in an argon or helium discharge are often of interest. When α_2 is small compared with α_1, Eq. (1) shows that ω_r is close to Ω_2, the cyclotron frequency of the "minor" species. For instance, if $M_1 = M_2$ but $Z_1 \neq Z_2$, Eq. (1) can be written

$$\omega_r^2 = \Omega_2^2\left(1 + \frac{n_2}{n_1}\right)\left[\left(1 + \frac{Z_2^2}{Z_1^2}\frac{n_2}{n_1}\right)\right]^{-1}, \qquad (2)$$

and the deviation of ω_r from Ω_2 is particularly sensitive to n_2/n_1 because of the weighting factor Z_2^2/Z_1^2.

Equation (1), however, is valid only for waves propagating exactly perpendicular to the dc magnetic field B_0; that is, for $k_\parallel = 0$. This is because ω_r is determined by the cancellation of the space charge of species l by that of species 2, without involvement of the electrons. Each ion species moves in elliptical orbits under the combined influence of the Lorentz force and the electrostatic E field of the wave; only at $\omega = \omega_r$ are the ellipses of equal width in the direction of $\mathbf{k}$. This balance is upset if $k_\parallel \neq 0$, so that electrons can move along $\mathbf{B}_0$ to cancel space charge. If $k_\parallel$ is sufficiently large—that is, if $k_\parallel^2/k_\perp^2$ is larger than m/M—the wave changes into the electrostatic ion-cyclotron wave, and the frequency shift then depends more on $k_\parallel$ than on n_2/n_1.

The shift caused by electron space charge depends critically on the mechanisms that control electron motion along $\mathbf{B}_0$: collisions with ions or neutrals, Landau damping, electron inertia, and the self-inductance of the parallel electron currents. Though not all of these mechanisms are effective at the same time, we have calculated all of them in Sec. II so as to allow this diagnostic to be used in a variety of circumstances. We have also, in the Appendix, calculated the effect of perpendicular electron drifts created by a density gradient.

The results of these calculations show that the electron motions would make this diagnostic useless unless $k_\parallel$ is so small as to be incompatible with any ordinary boundary conditions at the ends of the plasma column. On the other hand, the experimental data, shown in Sec. III, indicate that the resonance frequency, surprisingly, follows Eq. (1) almost exactly. To reconcile the observations with the theory, we have considered, in Sec. IV, the boundary conditions imposed by the sheaths on the endplates bounding the plasma. We find that, indeed, the sheaths require that $k_\parallel$ be extremely small as long as the wave suffers from a small amount of damping. Equations (1) and (2), therefore, can be used without correction in a wide range of parameters.

To detect a small percentage of a minor species, one merely has to excite a wave at a frequency close to Ω_2 and measure the exact frequency at which the largest plasma response is seen. Since Eq. (1) is obeyed only when $j_\parallel$ vanishes, we suggest an extension of the method that can yield the *local* impurity concentration. By using a double-sided probe to measure $j_\parallel$, the frequency at which $j_\parallel = 0$ can be found as a function of position; and the spatial variation of n_2/n_1 can, in principle, be obtained.

II. THE ELECTROMAGNETIC DISPERSION RELATION

We consider waves in an infinite, uniform plasma with $T_i = 0$ and $\mathbf{B} = B\hat{z}$ that propagate in the yz plane, so that $k^2 = k_y^2 + k_z^2$, with $k_z^2 \ll k_y^2$ and $k_x = 0$. Neglecting the displacement current in Maxwell's equations, we obtain in standard fashion[2,3] a wave equation whose components are

$$k^2 E_x = (4\pi i\omega/c^2) j_x\,, \qquad (3)$$

$$k_z^2 E_y - k_y k_z E_z = (4\pi i\omega/c^2) j_y\,, \qquad (4)$$

$$k_y^2 E_z - k_z k_y E_y = (4\pi i\omega/c^2) j_z\,. \qquad (5)$$

The perpendicular currents j_x and j_y are easily found[2,3] from the cold-ion equations of motion and from the electron

[a] Permanent address: Electrical Engineering Department, University of California, Los Angeles, California 90024.

 0031-9171/86/051651-08$01.90 © 1986 American Institute of Physics

$\mathbf{E}\times\mathbf{B}$ drifts, since electron thermal and inertial effects are negligible in $j_\perp$. Eqs. (3) and (4) can then be written

$$[\kappa^2 + f(\Omega)]E_x + ig(\Omega)E_y = 0, \tag{6}$$

$$-ig(\Omega)E_x + [\kappa_z^2 + f(\Omega)]E_y - \kappa_y\kappa_z E_z = 0, \tag{7}$$

where, if there are two ion species,

$$f(\Omega) = \{\alpha_1/[1-(R\Omega)^{-2}]\} + [\alpha_2 R/(1-\Omega^{-2})], \tag{8}$$

$$g(\Omega) = R\Omega[\alpha_1/(R^2\Omega^2-1) + \alpha_2/(\Omega^2-1) + 1]. \tag{9}$$

Here we have used the dimensionless parameters

$$\Omega \equiv \omega/\Omega_2, \qquad R \equiv \Omega_2/\Omega_1, \qquad \kappa = kL_i, \tag{10}$$

$$\alpha_j \equiv Z_j n_{oj}/n_{oe}, \qquad \Omega_j = Z_j eB/M_j c, \tag{11}$$

$$L_i \equiv (M_i c^2/4\pi Z_i n_{oe} e^2)^{1/2} \simeq c/\Omega_{pi}, \tag{12}$$

and it is understood that the major species is 1 and the minor species is 2. In this notation, the Buchsbaum formula [Eq. (1)] is simply $f(\Omega) = 0$.

To calculate the frequency shift caused by finite k_z, we must evaluate j_z in Eq. (5) including the effects of inertia, collisions, and Landau damping on the electron parallel motion. To do this, we solve the Vlasov equation with a Krook collision term to obtain v_z for the electrons:

$$\frac{\partial f_1}{\partial t} + v_z\frac{\partial f_1}{\partial z} - \frac{e}{m}E_z\frac{\partial f_0}{\partial v_z} = \nu_e\left(\frac{n_1}{n_0}f_0 - f_1\right). \tag{13}$$

for $k_z^2 \ll k_y^2$, the contribution of ion v_z to j_z may be neglected. Using the electron continuity equation for n_1, we obtain

$$\frac{4\pi i\omega}{c^2}j_z = -\frac{\omega_p^2}{c^2}Z'(\zeta) \times\frac{(\omega/k_z v_{\rm th})\zeta E_z + (\nu_e/2\omega_c)(k_y/k_z)E_x}{1-(i\nu_e/2\omega)Z'(\zeta)}, \tag{14}$$

where

$$\zeta \equiv (\omega + i\nu_e)/k_z v_{\rm th}, \qquad v_{\rm th}^2 = 2kT_e/m, \tag{15}$$

$Z'(\zeta)$ is the derivative of the plasma dispersion function,[4] and ν_e is an approximate collision frequency for electrons against either ions or neutrals. The term containing ν_e/ω_c in the numerator of Eq. (14) can safely be neglected. Using Eq. (14) in Eq. (5), one obtains

$$-\kappa_y\kappa_z E_y + (\kappa_y + P)E_z = 0, \tag{16}$$

where

$$P \equiv \frac{M_1}{Z_1 m}\frac{\zeta\,\mathrm{Re}(\zeta)Z'(\zeta)}{\{1-(i/2)(\nu_e/\omega)Z'(\zeta)\}}. \tag{17}$$

A solution of Eqs. (6), (7), and (16) is possible if the determinant of the coefficients vanishes. This condition yields the despersion relation for electromagnetic two-ion hybrid waves:

$$f(\Omega) = -\frac{P\kappa^2\kappa_z^2 + (f^2-g^2)(P+\kappa_y^2)}{P(\kappa^2+\kappa_z^2) + \kappa^2\kappa_y^2}. \tag{18}$$

We next show that this equation reduces to well-known results in limiting cases. The electromagnetic ion-cyclotron wave in a single ion species plasma can be obtained by letting $\alpha_2 = 0$, $\alpha_1 = 1$, $R = 1$, and $P\to\infty$. The dimensionless parameter P is proportional to the parallel electron flow, so that when P is large, the electric field E_z is shorted out, as shown by Eq. (16). In this limit, Eq. (18) becomes

$$f(\kappa^2+\kappa_z^2) = g^2 - f^2 - \kappa^2\kappa_z^2, \tag{19}$$

where $f = \Omega^2/(\Omega^2-1)$ and $g = \Omega f$. This yields

$$\Omega^2 = \left(1 + \frac{1}{\kappa_z^2} + \frac{1}{\kappa^2} - \frac{\Omega^4}{\kappa^2\kappa_z^2}\right)^{-1}. \tag{20}$$

When $\Omega \simeq 1$ and $\kappa^2 \gg 1$, ($\lambda_\perp/2\pi < c/\Omega_p$), the last term can be neglected, and Eq. (20) becomes the Stix dispersion relation[3]

$$\omega^2 = \Omega_c^2\left[1 + \frac{\Omega_p^2}{c^2}\left(\frac{1}{k_z^2} + \frac{1}{k^2}\right)\right]^{-1}. \tag{21}$$

The electrostatic limit is obtained by letting $c\to\infty$, so that L_i, κ, and κ_z all approach ∞. Keeping only the κ^4 terms in Eq. (18), we obtain

$$f(\Omega) = -P(k_z^2/k_y^2). \tag{22}$$

This is the dispersion relation for *electrostatic* two-ion hybrid waves with finite k_z. When $k_z = 0$, this becomes $f(\Omega) = 0$, which is identical with Eq. (1).

With some care, the electrostatic ion-cyclotron (ESIC) wave can also be obtained from Eq. (22). In that wave, k_z^2 is much smaller than k_y^2, but is still large enough to permit sufficient electron motion along $\mathbf{B}$ for the electron Boltzmann relation to hold. This physical situation can be described formally by taking the limit $m\to 0$, so that $\zeta\to 0$. Using the power series expansion of $Z'(\zeta)$,

$$Z'(\zeta) = -2i\sqrt{\pi}\,\zeta e^{-\zeta^2} - 2 + 4\zeta^2 + \cdots \simeq -2, \tag{23}$$

in Eq. (17) and inserting into Eq. (22), we obtain for $\nu_e = 0$,

$$f(\Omega) = 2\zeta^2\frac{M_1}{Z_1 m}\frac{k_z^2}{k_y^2} = \frac{\Omega^2}{\kappa_z^2}\left(\frac{Z_2 M_1}{Z_1 M_2}\right)^2\frac{2}{\beta_e}, \tag{24}$$

where $\beta_e = 8\pi n_{0e}kT_e/B^2$. When there are two ion species, Eq. (24) gives the ESIC wave for each species as modified by the presence of the other. When there is only one ion species, Eq. (24) becomes

$$\omega^2 = \Omega_c^2 + k_y^2 c_s^2, \quad c_s^2 = ZkT_e/M, \tag{25}$$

which is the usual ESIC relation.[5]

In the experiment to be described, $|\zeta|$ is of order 20; and it is appropriate to use the asymptotic expansion for $Z'(\zeta)$:

$$Z'(\zeta) = \frac{1}{\zeta^2} + \frac{3}{2}\frac{1}{\zeta^4} + \cdots \simeq \frac{1}{\zeta^2}. \tag{26}$$

A good approximation for P [Eq. (17)] is then given by

$$P \simeq \frac{M_1/Z_1 m}{(1+i\nu_e/\omega)(1-i\nu_e/2\omega\zeta^2)} \simeq \frac{M_1/Z_1 m}{1+i\nu_e/\omega}. \tag{27}$$

In this case, Landau damping is completely negligible. For real k_z and complex ω, the frequency shift can be calculated by expanding around the $k_z = 0$ resonance frequency ω_r. Let the frequency shift be $\epsilon\omega_r$, so that

$$\Omega = \Omega_r(1+\epsilon), \tag{28}$$

where $\epsilon \ll 1$. Since Ω_r is defined by $f(\Omega_r) = 0$, the left-hand side of Eq. (18) is given by

$$f(\Omega) = \epsilon\Omega_r[f'(\Omega)]_{\Omega=\Omega_r}. \tag{29}$$

A little algebra yields

$$f(\Omega) = -\frac{2\epsilon}{\Omega_r^2}\frac{\alpha_1^2}{\alpha_2}\frac{[R+(\alpha_2/\alpha_1)]^3}{(1-R^2)^2}. \tag{30}$$

On the right-hand side of Eq. (18), the term in (f^2-g^2) can be shown to be negligible, as is κ_z^2 relative to κ^2. With the use of Eq. (27), we then have for Eq. (18),

$$f(\Omega) \simeq -\frac{\kappa_z^2}{1+(c^2k^2/\omega_p^2)(1+i\nu_e/\omega_2)}. \tag{31}$$

The last two equations give the frequency shift

$$\delta\Omega = \epsilon\Omega_r = \frac{\alpha_2\Omega_r^3(1-R^2)^2}{2\alpha_1^2[R+(\alpha_2/\alpha_1)]^3} \times \frac{\kappa_z^2}{1+(c^2k^2/\omega_p^2)(1+i\nu_e/\omega_r)}. \tag{32}$$

On the other hand, if we take ω to be real and k_z complex, Eq. (18) can be rearranged to give

$$\kappa_z^2 = -\frac{\kappa_y^2 f + f^2 - g^2}{f+\kappa_y^2}\left(1+\frac{\kappa_y^2}{P}\right), \tag{33}$$

where again we have neglected κ_z^2 relative to κ_y^2. With P approximated by Eq. (37), it is independent of κ_z; and Eq. (33) becomes

$$\kappa_z^2 = \frac{g^2-f^2-f\kappa_y^2}{f+\kappa_y^2} \times\left[1+\frac{Z_1 m}{M_1}\kappa_y^2\left(1+\frac{i\nu_e}{\omega}\right)\right]. \tag{34}$$

Eqs. (32) and (34) will be used in analyzing the data.

III. EXPERIMENT AND INITIAL ANALYSIS

The experiment, whose results were reported earlier,[6] was done in a linear discharge produced by volume ionization of an argon–xenon mixture. The plasma column was 9 cm in diameter and 150 cm long, in a magnetic field B_0 of 10.23 kG, uniform to $\pm 0.7\%$. The major species was argon at a pressure p of 4×10^{-4} Torr, and the minor species was xenon at a variable pressure $p<3\times10^{-5}$ Torr. The plasma density was $n = 2.2\times10^{11}\,\mathrm{cm}^{-3}$, and the temperatures were $KT_e \simeq 3$ eV, $KT_i = 0.2-0.4$ eV.

The plasma is produced at one end by 10 kW of 100 MHz rf applied to a 10×10 cm electrode structure consisting of horizontal tantalum strips 1 cm apart, viewed edge-on along the field lines, with every other strip connected to the same terminal of the rf source. Primary electrons accelerated by the rf field travel along **B** to ionize the background gas. These primaries do not produce any turbulence in the ion-cyclotron range of frequencies. The plasma is terminated at the other end by a metal plate biased at 60 V relative to ground; this endplate determines the plasma potential, which is slightly positive with respect to the endplate because of the usual anode sheath formation. To excite the two-ion resonances, the endplate is split along a diameter and the gap closed by overlapping the D-shaped halves. An ac voltage of variable frequency and 60 V peak-to-peak amplitude is applied across the halves to excite the waves.

The plasma resonances are detected with a radial energy analyzer[7] (REA), which consists of a flat 0.018 cm^2 collector recessed in a tube and oriented so that its normal and the tube axis are perpendicular to $\mathbf{B}_0$. The setback is adjusted so that electrons, with $r_L \simeq 10^{-3}$ cm, cannot reach the collector, while ions, with $r_L > 0.05$ cm, can. The collector can be biased positively for energy discrimination.

The presence of a cyclotron-type wave in the plasma is detected by the REA current, which consists of ions accelerated by the $\mathbf{E}_\perp$ of the wave to an energy high enough to overcome the collector bias. Examples of resonance curves are shown in Fig. 1 for various relative xenon concentrations α_2/α_1. A peak in REA current is found at an excitation frequency, which varies from the ^{131}Xe gyrofrequency of 119 kHz toward the ^{40}Ar gyrofrequency of 390 kHz as α_2/α_1 is increased, as predicted by Eq. (1). These resonances have widths of order 6% caused by collisional broadening, so that the individual isotopes of Xe with mass differences of order 4% are not resolvable. Figure 2 shows the variation of REA current with collector bias for various α_2/α_1. The straight-line behavior on the semilog plot indicates a Maxwellian ion distribution in each case. The ion temperature decreases as α_2/α_1 increases, in agreement with the physical picture that the minority ions then need smaller $v_\perp$ to cancel the space charge of the majority species.

The absolute Xe density can also be obtained from Fig. 2 by using the formula for random ion current density at the plasma potential,

$$J(V_p) = \tfrac{1}{4}ne\bar{v} = ne(KT_i/2\pi M)^{1/2}, \tag{35}$$

using the measured T_i, and extrapolating to $V_p = 92$ V. The accuracy of this method was checked in an ^{40}Ar plasma containing an ^{36}Ar minority. The ^{40}Ar density was essentially the same as n_e, and the latter was measured with a Langmuir probe calibrated with microwave interferometry, as well as by the characteristics of resonance cones.[8] Using an REA and Eq. (35), we found the density ratio of ^{36}Ar to ^{40}Ar was within 30% of the natural abundance of 0.3%.

Figure 3 shows the frequency shift $\Omega - 1$ [i.e., $[(\omega-\Omega_{Xe})/\Omega_{Xe}]$ versus relative resonance frequency

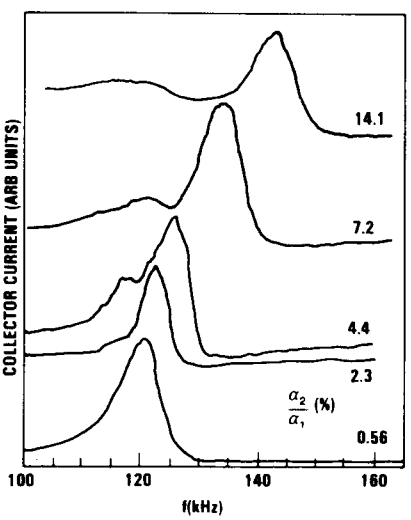

FIG. 1. Current to the radial energy analyzer at fixed bias versus drive frequency for various concentrations of the minority species, as determined by the partial pressure of xenon in a Xe–Ar mixture.

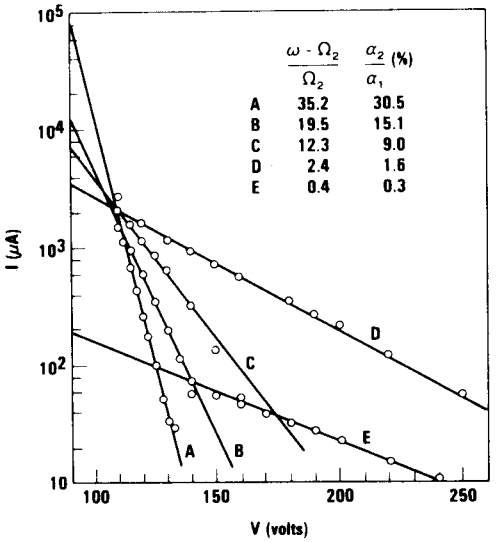

FIG. 2. Radial energy analyzer current at the resonance peak versus retarding potential for various relative xenon concentrations and corresponding frequency shifts. The plasma potential is 92 V.

computed from Eq. (1). It is seen that this simple formula, surprisingly, fits the data within the experimental error.

Since the experiment was done in a finite-length plasma, one would expect agreement with the finite-k_z formula equation (18) or the approximation to it, Eq. (32). The numerical parameters of the experiment are as follows:

$$
\begin{aligned}
&a = 4.5 \text{ cm}, && k_y = m/r \simeq 0.44 \text{ cm}^{-1},\\
&L = 150 \text{ cm}, && \kappa_y = 135,\\
&\Omega_1 = 2.45\times 10^6 \text{ sec}^{-1}, && \Omega_2 = 7.49\times 10^5 \text{ sec}^{-1},\\
&v_{th} = 1.03\times 10^8 \text{ cm/sec}, && \nu_e = 1.9\times 10^6 \text{ sec}^{-1},\\
&\Omega_{pi} = 9.77\times 10^7 \text{ sec}^{-1}, && L_i = 306.8 \text{ cm},\\
&R = 0.305, && \nu_e/\Omega_2 = 2.5,
\end{aligned}
\tag{36}
$$

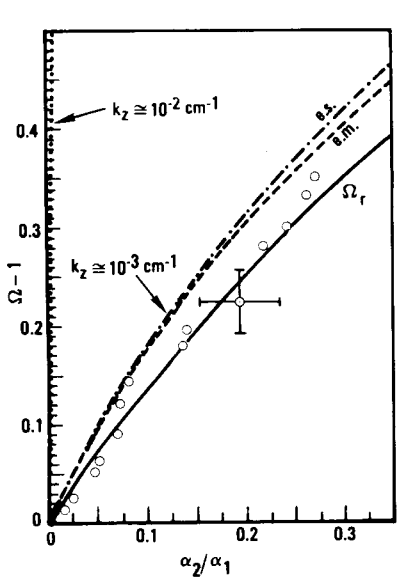

FIG. 3. Frequency shift relative to the xenon gyrofrequency versus the xenon/argon density ratio. The solid curve is the two-ion hybrid frequency shift for $k_\parallel = 0$. The other curves are theoretical predictions for finite $k_\parallel$ (see text).

Here L is the length of the plasma, and L_i the ion skin depth. The value of k_y is computed for an $m = 2$ azimuthal mode, as the exciter geometry suggests. The electron collision frequency ν_e is taken to be the sum of the electron-argon collision rate $\nu_{e0} = 4.2\times 10^5 \text{ sec}^{-1}$ at 3 eV and the electron–ion collision rate $\nu_{ei} = 1.5\times 10^6 \text{ sec}^{-1}$ at 3 eV and 2.2×10^{11} cm^{-3} density.

What is not certain is the value of k_z. If one assumes that the wave has a quarter-wavelength between the conducting endplates, then $k_z = \pi/2L$, and we have

$$
\begin{aligned}
&k_z = 1.05\times 10^{-2} \text{ cm}^{-1}, \quad k_z^2/k_y^2 = 5.55\times 10^{-4},\\
&|\mathrm{Re}\,\zeta| \simeq 0.7, \quad |\mathrm{Im}\,\zeta| \simeq 1.76,
\end{aligned}
\tag{37}
$$

With these values, solution of Eq. (18) yields the dotted line on Fig. (3), which is very close to the vertical axis. With such a large value of k_z, electron conduction along **B** completely destroys the two-ion hybrid effect, and Eq. (1) is not even approximately correct.

We have pointed out previously,[9] however, that ion sheaths can absorb most of the potential drop at the endplates, allowing the wave to have a finite amplitude at the sheath edge. Normal modes satisfying the sheath boundary conditions can then have effective wavelengths much longer than L. A more recent calculation[10] exhibited several normal modes of different symmetry appropriate to single-ended drive. All of these modes have an effective value of k_z given by

$$
k_z = \left(\frac{a\nu_e L}{\pi}\right)^{1/2}\frac{4}{L}, \quad a = \frac{m v_B}{KT_e}, \quad v_B = \frac{1}{2}\left(\frac{KT_e}{M_1}\right)^{1/2},
\tag{38}
$$

in the collision-dominated case. For our experiment, this yields an order of magnitude reduction in k_z:

$$
k_z = 9.05\times 10^{-4} \text{ cm}^{-1}, \quad |\mathrm{Re}\,\zeta| \simeq 8, \quad |\mathrm{Im}\,\zeta| \simeq 20. \tag{39}
$$

For such large $|\zeta|$, Eq. (27) is valid; and using this in Eq. (18) or using Eq. (32) yields the dashed curve in Fig. 3. Though that curve is much closer to the data, it is still outside the experimental error. More important, it lies far enough from the $k_z = 0$ curve so that the use of this method as an impurity diagnostic would entail the difficult evaluation of a finite $-k_\parallel$ correction.

The dot-dash curve on Fig. 3 is the result of making the electrostatic assumption, Eq. (22). The apparent agreement with the electromagnetic solution is fortuitous, as we show in Fig. 4. Here we have studied the effect of varying ν_{ei} and k_z independently, assuming that they are not related by Eq. (38). It is seen that the electrostatic and electromagnetic solutions agree only near the actual value of ν_e, indicated by the circle. This graph shows the sensitivity of $\Omega - 1$ to k_z and that, for $k_z \simeq 10^{-3}$ cm^{-1}, agreement with experiment is achieved only if ν_e is anomalously large by a factor greater than 5.

IV. IMPROVED SHEATH BOUNDARY CONDITIONS

Different types of endplate boundary conditions are shown in Fig. 5. In (A), the wave has nodes at the endplates if there is no sheath or a highly conducting (electron-rich)

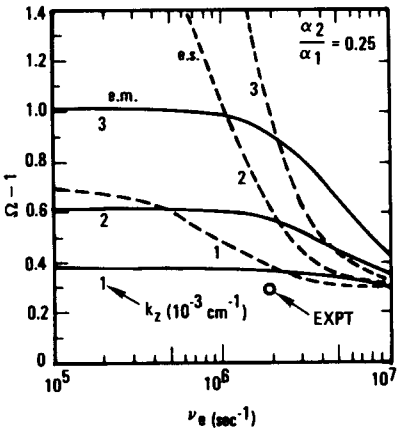

FIG. 4. Relative frequency shift at $\alpha_2/\alpha_1 = 0.25$ versus electron collision frequency ν_e for three values of k_z. The solid lines are the electromagnetic dispersion relation, and the dashed lines the electrostatic approximation.

sheath. In (B), a symmetric mode with $\lambda_z \gg L$ can exist if the sheaths are good enough insulators to absorb the potential drop; this diagram assumes small or zero $\mathrm{Im}(k_z)$. In (C), we show the case $\mathrm{Im}(k_z) \gg \mathrm{Re}(k_z)$, with the wave excited at the right and damped as it propagates to the left. Case (B) was treated previously,[9,10] and we now adapt the theory to case (C).

The conditions near an endplate are sketched in Fig. 6. Let the sheath be ion-rich, so that the potential $\phi(z)$ has the slope shown and the electrons are repelled by the Coulomb barrier while the ions are accelerated into the endplate. The inward particle fluxes are then given by

$$\Gamma_e = n v_r \exp(-e\phi/kT_e)\,, \tag{40}$$

$$\Gamma_i = n v_B\,, \tag{41}$$

where v_r is the random velocity and v_B the Bohm (presheath) velocity given by

$$v_r = (KT_e/2\pi m)^{1/2}\,, \tag{42}$$

$$v_B \simeq 0.5(KT_e/M)^{1/2}\,. \tag{43}$$

In equilibrium, the plasma potential ϕ_0 is fixed by the condition $\Gamma_i = \Gamma_e$, so that $e\phi_0/KT_e = \ln(v_r/v_B)$. We now assume that a wave perturbs the density and potential at the

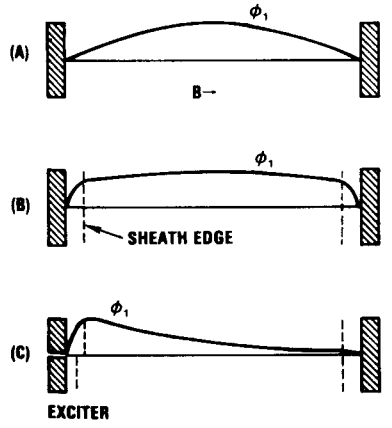

FIG. 5. Schematic of axial wave amplitude variation with different sheath boundary conditions and wave damping.

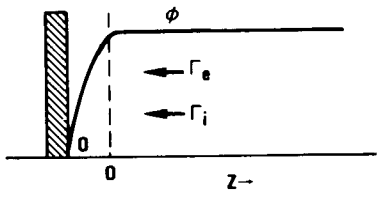

FIG. 6. Schematic of the potential and particle fluxes near the sheath edge (dashed line) of a grounded endplate.

sheath edge so that $n = n_0 + n_1$, $\phi = \phi_0 + \phi_1$. These fluctuations will be too fast to affect Γ_i, which is established in the large presheath region; but Γ_e will fluctuate, causing a net current through the sheath. Linearizing Eq. (40) about $\Gamma_{e0} = n_0 v_B$, we obtain

$$\Gamma_{e1} = n_0 v_B(\nu - \chi)\,, \tag{44}$$

where

$$\nu \equiv n_1/n_0, \quad \chi \equiv e\phi_1/KT_e\,. \tag{45}$$

If v_z is the perturbation in electron fluid velocity, then Γ_{e1} corresponds to a velocity $v_z = \pm \Gamma_{e1}/n_0$, the top (bottom) sign referring to the right (left) endplate. Thus, if n_1, ϕ_1 at the sheath edge are given, sheath balance fixes the value of v_z. By identifying this value of v_z with the v_z of the *wave* at that point, we can obtain the effective value of k_z.

The electron equation of motion for v_z in the absence of Landau damping is

$$mn_0 \frac{\partial v_z}{\partial t} = en_0 \frac{\partial \phi_1}{\partial z} - KT_e \frac{\partial n_1}{\partial z} - mn_0 \nu_e v_z\,, \tag{46}$$

$$\frac{\partial v_z}{\partial t} = \frac{KT_e}{m}(\chi - \nu)' - \nu_e v_z\,. \tag{47}$$

From Eq. (44), we have

$$v_z = \pm v_B(\nu - \chi)\,. \tag{48}$$

Defining

$$\psi \equiv \nu - \chi\,, \tag{49}$$

$$a \equiv m v_B/KT_e\,, \tag{50}$$

we can write Eqs. (47) and (48) as

$$\frac{\partial \psi}{\partial z} \pm a\frac{\partial \psi}{\partial t} \pm a\nu_e \psi = 0\,. \tag{51}$$

This is the sheath matching condition for the right and left endplates, respectively.

Let the sheath edges be at $z = 0$ and L, and let the exciter be on the left, as in Fig. 5(c). If the driven endplate has potential ϕ_p, then the sheath drop is $\phi - \phi_p$, and Eq. (48) should be replaced by $v_z = -v_B(\nu - \chi + \chi_p) = -v_B(\psi + \chi_p)$. Using this value in Eq. (47) for $z = 0$ and setting $\chi_p = 0$ for the undriven endplate at $z = L$, we obtain the boundary conditions

$$\frac{\partial \psi}{\partial z} - a\frac{\partial}{\partial t}(\psi + \chi_p) - a\nu_e(\psi + \chi_p) = 0\,, \quad \text{at } z = 0\,, \tag{52}$$

$$\frac{\partial \psi}{\partial z} + a\frac{\partial \psi}{\partial t} + a\nu_e \psi = 0, \quad \text{at } z = L\,. \tag{53}$$

The wave variables ν and χ have the usual $\exp[i(k_y y$

$+k_z z-\omega t)]$ dependence, but they must satisfy Eqs. (52) and (53) at $z=0,L$. The method of excitation calls for real ω and k_y and complex k_z of the form

$$k_z=\beta+i\alpha\,. \tag{54}$$

Since the driver is at $z=0$, we look for solutions of the form

$$\psi=A(t)+B(t)e^{-\alpha z}\cos\beta z\,. \tag{55}$$

Let the exciter voltage have the form

$$\chi_p=\chi_m\cos\phi,\quad \phi\equiv\omega t-k_\perp y\,. \tag{56}$$

The functions $A(t)$ and $B(t)$, which allow for different time-varying sheath drops at the two ends, will also vary sinusoidally with ϕ, and hence will have the form

$$\begin{aligned}A(t)&=a_1\cos\phi+a_2\sin\phi\,,\\ B(t)&=b_1\cos\phi+b_2\sin\phi\,.\end{aligned} \tag{57}$$

Substituting Eqs. (55) and (57) into (52) and (53) and equating the coefficients of $\sin\phi$ and $\cos\phi$, we obtain four simultaneous equations for the constants a_1, a_2, b_1, and b_2:

$$\begin{aligned}&a_2+b_2+Db_1+C(a_1+b_1+\chi_m)=0\,,\\ &C(a_2+b_2)+Db_2-(a_1+b_1+\chi_m)=0\,,\\ &a_2+b_2F-Gb_1+C(a_1+b_1F)=0\,,\\ &C(a_2+b_2F)-Gb_2-(a_1+b_1F)=0\,.\end{aligned} \tag{58}$$

Here we have introduced the abbreviations

$$\begin{aligned}&C\equiv\nu_e/\omega\,,\quad D\equiv\alpha/a\omega\,,\\ &F\equiv e^{-\alpha L}\cos\beta L\,,\\ &G\equiv(\alpha\cos\beta L+\beta\sin\beta L)e^{-\alpha L}/a\omega\,.\end{aligned} \tag{59}$$

After some algebra, we obtain the following solution:

$$\begin{aligned}a_1&=\mathbf{D}^{-1}\chi_m\,[CF(D+2G)-G(C+D+G)\\ &\quad+F(1-F)(1+C^2)]\,,\\ a_2&=-\mathbf{D}^{-1}\chi_m(G+DF)\,,\\ b_1&=-\mathbf{D}^{-1}\chi_m[(C(D+G)+(1-F)(1+C^2)]\,,\\ b_2&=\mathbf{D}^{-1}\chi_m(D+G)\,,\\ \mathbf{D}&=(D+G)^2\\ &\quad+2C(1-F)(D+G)+(1-F)^2(1+C^2)\,,\end{aligned} \tag{60}$$

Let the detector be located at $z=d$, and let F_d be defined as $F_d=e^{-\alpha d}\cos\beta d$ The wave amplitude ψ at the detector is then

$$\psi(d)=(a_1+b_1F_d)\cos\phi+(a_2+b_2F_d)\sin\phi\,, \tag{61}$$

with the coefficients given by Eq. (60) as functions of ω, α, and β.

In general, none of these coefficients vanishes, so that the simplest mode that satisfies the matching conditions at both sheaths is, from Eq. (55), a combination of the lowest k_z mode and the $k_z=0$ mode. The relative amplitudes and phases of these modes is fixed by the boundary conditions. Furthermore, for the finite-k_z part, both α and β are given as functions of ω by the dispersion relation of Eq. (34).

V. RESULTS AND DISCUSSION

Our computational procedure is as follows. The experimental conditions specify the parameters given in Eq. (36). For each value of α_2/α_1, a value of $\Omega(=\omega/\Omega_2)$ is guessed. The functions f and g can then by evaluated, and κ_z is found from Eq. (34), yielding α and β. The quantities C, D, F, and G are then specified by Eq. (59), and then $a_{1,2}$ and $b_{1,2}$ are given by Eq. (60) in terms of χ_m. Inserting the probe position (typically, $d=L/2$), we can then compute $|\psi/\chi_m|\equiv\mathbf{N}/\mathbf{D}$ as a function of Ω and α_2/α_1.

Figure 7 shows the results for $\alpha_2/\alpha_1=0.25$. The Buchsbaum resonance frequency Ω_r for this case is 1.299956. It is seen that the plasma response $|\Omega/\chi_m|$ peaks immeasurably close to $\Omega=\Omega_r$, in agreement with observations. We now give a possible physical reason for this. The values of $\alpha=\mathrm{Im}\,k_z$ and $\beta=\mathrm{Re}\,k_z$ are shown for this case as functions of $\Omega-1$ in Fig. 8. It is seen that the dispersion relation requires α to be two orders of magnitude larger than β for the value of ν_e that we used. From this it is clear that the current into the sheath is controlled by the damping length rather than the wavelength. Because of the relatively large value of $|k_z|$, this current would be more than the sheath can conduct unless the oscillation is one that causes very little parallel current; such an oscillation is precisely the classical two-ion hybrid at $\Omega=\Omega_r$.

The value of ν_e/ω in this experiment was $\simeq 2.5$. Figure 8 shows that the damping length can be increased two orders of magnitude before $\mathrm{Re}\,(k_z)$ becomes comparable to $\mathrm{Im}(k_z)$, in which case the shift from $\Omega=\Omega_r$ can become appreciable, as can be seen from the dashed curve of Fig. 3. Thus, it is possible to neglect the finite-k_z frequency shift over a large range of collisionalities, and this diagnostic technique has wide applicability. If ν_e/ω should be much larger than 1, it would be possible to neglect the time-derivative terms in Eqs. (52) and (53), thus reducing the algebraic complexity. However, the result would be the same: $\Omega=\Omega_r$ is a good approximation. We have tried other forms for $\psi(z,t)$ in place of Eq. (55), but no simpler form is capable of satisfying the dispersion relation and both sheath conditions.

In deriving the sheath conditions, Eqs. (52) and (53), we neglected Landau damping and the effect of B_1 on the

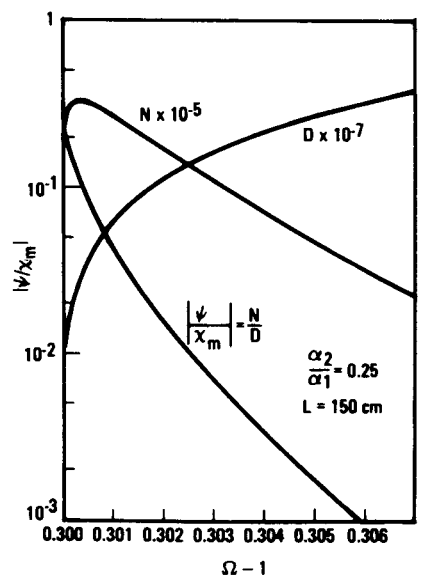

FIG. 7. Normalized wave amplitude $|\psi/\chi_m|$ versus frequency shift $\Omega-1$, computed for the parameters of the experiment and $\alpha_2/\alpha_1=0.25$.

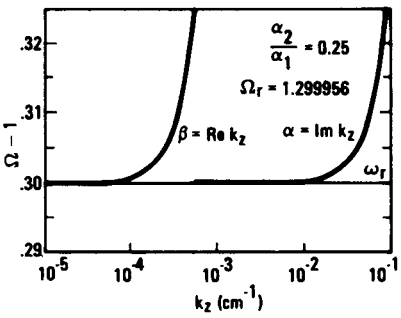

FIG. 8. Real and imaginary parts of k_z vs $\Omega - 1$ for $\alpha_2/\alpha_1 = 0.25$.

electron motion. The latter omission is justified, since B_1 enters only in Lorentz force, which is perpendicular to v_z. However, in cases where Landau damping is stronger than collisional damping, the sheath conditions would have to be recalculated.

ACKNOWLEDGMENTS

We are indebted to Dr. J. J. Thomson for suggesting the theoretical examination of this problem and for helpful comments, and to M. Mussetto and M. Makowski for communicating other experimental data that confirm the usefulness of this diagnostic.

APPENDIX: THE TWO-ION HYBRID WAVE IN AN INHOMOGENEOUS PLASMA

We make the electrostatic approximation at the outset and consider an equilibrium with $T_i = 0$ and a density gradient that is the same for all species:

$$\delta \equiv n_{0j}'/n_{0j} ,$$

where the prime indicates $\partial/\partial x$. Here ∇n_0 is in the x direction, $\mathbf{B}_0$ is in the z direction, and $\mathbf{k}$ is in the yz plane. Following the usual treatment of resistive drift waves,[11] we consider the electrons to be a warm, isothermal, massless fluid with parallel resistivity $\eta_\parallel$ described by the equation of motion

$$en_e(-\nabla\phi + \mathbf{v}_e \times \mathbf{B}_0) + KT_e \nabla n_e + n_e^2 e^2 \eta_\parallel v_{ez}\hat{z} = 0 , \quad \text{(A1)}$$

where

$$\eta_\parallel = m\nu_{ei}/n_0 e^2 . \quad \text{(A2)}$$

In the η term, we have neglected the effect of $\eta_\perp$ on $\mathbf{v}_{e\perp}$ and of v_{iz} on the parallel electron drag. Linearizing about an equilibrium with

$$\mathbf{v}_{0e} = -D_B \delta \hat{y} \equiv v_D \hat{y} , \quad \text{(A3)}$$

where D_B is the Bohm diffusion coefficient

$$D_B = cKT_e/eB_0 , \quad \text{(A4)}$$

we Fourier analyze and solve Eq. (A1) to obtain

$$\begin{aligned} iv_{ex} &= k_y D_B(\chi - \nu) , \\ v_{ey} &= D_B(\chi - \nu)' , \\ v_{ez} &= ik_z D_B \omega_c \tau_{ei}(\chi - \nu) , \end{aligned} \quad \text{(A5)}$$

where $\tau_{ei}^{-1} = \nu_{ei} = \nu_e$. Here the density and potential are normalized as follows:

$$\nu \equiv n_{ie}/n_{0e}(x), \quad \chi \equiv e\phi_1/KT_e . \quad \text{(A6)}$$

Substituting into the linearized equation of continuity,

$$\begin{aligned} &-i(\omega - k_y v_D)n_{1e} + v_{ex} n_{0e}' \\ &\quad + n_{0e}(v_{ex}' + ik_y v_{ey} + ik_z v_{ez}) = 0 , \end{aligned} \quad \text{(A7)}$$

and defining

$$\begin{aligned} &\omega_* \equiv k_y v_D , \quad a_i^2 \equiv KT_e/M\Omega_c^2 \\ &b \equiv k_y^2 a_i^2, \quad \sigma_\parallel \equiv (k_z/k_y)^2 \omega_c \tau_{ci} \Omega_c , \end{aligned} \quad \text{(A8)}$$

we obtain a modified Boltzmann relation between ν and χ:

$$\nu/\chi = (\omega_* + ib\sigma_\parallel)/(\omega + ib\sigma_\parallel) . \quad \text{(A9)}$$

This is the collisional limit of the more general expression

$$\frac{\nu}{\chi} = \frac{1 + [(\omega + i\nu_e - \omega_*)/k_z v_{th}]Z(\zeta)}{1 + (i\nu_e/k_z v_{th})Z(\zeta)} , \quad \text{(A10)}$$

which can be found by solving the drift-kinetic equation[12]

$$\begin{aligned} &\frac{\partial f_1}{\partial t} + v_z \frac{\partial f_1}{\partial z} + \frac{E_y}{B}\frac{\partial f_0}{\partial x} + \frac{q}{m}E_z \frac{\partial f_0}{\partial v_z} \\ &\quad = \nu_e [(n_1/n_0)f_0 - f_1] . \end{aligned} \quad \text{(A11)}$$

For each cold-ion species j, the velocity components corresponding to Eq. (A5) are

$$\begin{aligned} iv_{jx} &= D_B[k_y\chi - (\omega/\Omega_j)\chi'](1 - \omega^2/\Omega_j^2)^{-1} , \\ v_{jy} &= D_B[\chi' - (\omega/\Omega_j)k_y\chi](1 - \omega^2/\Omega_j^2)^{1} . \end{aligned} \quad \text{(A12)}$$

The ion parallel motion v_{jz} can be neglected because of the small values of k_z^2/k_y^2 here. The equation of continuity is

$$-i\omega n_j + v_{jx} n_{0j}' + n_{0j}(v_{jx}' + ik_y v_{jy}) = 0 . \quad \text{(A13)}$$

Substituting Eqs. (A5), (A7), (A12), and (A13) into the quasineutrality condition $n_e = \Sigma_j Z_j n_j$ then yields

$$\begin{aligned} \nu = D_B &\sum_j \frac{\alpha_j}{\Omega_j^2}\left(1 - \frac{\omega^2}{\Omega_j^2}\right)^{-1} \\ &\times\{\chi'' + \delta\chi' - [k_y^2 + k_y\delta(\Omega_j/\omega)]\chi\} = 0 , \end{aligned} \quad \text{(A14)}$$

where the definitions of Eqs. (11) and (A6) have been used. Equating this value of ν to that of Eq. (A10) for electron motions and defining the acoustic velocities

$$c_{sj}^2 \equiv Z_j KT_e/M_j , \quad \text{(A15)}$$

we obtain the following dispersion equation for multispecies ion hybrid or electrostatic ion-cyclotron waves in a density gradient n_0'/n_0:

$$\begin{aligned} &\sum_j \frac{\alpha_j c_{sj}^2}{\omega^2 - \Omega_j^2}\left[\frac{\chi''}{\chi} + \frac{n_0'}{n_0}\frac{\chi'}{\chi} - k_y\left(k_y + \frac{\Omega_j}{\omega}\frac{n_0'}{n_0}\right)\right] \\ &\quad + \frac{1 + [(\omega + i\nu_e - \omega_*)/k_z v_{th}]Z(\zeta)}{1 + (i\nu_e/k_z v_{th})Z(\zeta)} = 0 . \end{aligned} \quad \text{(A16)}$$

To make further progress, it is customary to make the "local" approximation and set $\chi'' = \chi' = 0$. If we do this and specialize to the case of two-ion species and collision-dominated electron parallel motion, we obtain

$$\begin{aligned} &\frac{\alpha_1\Omega_1}{\omega^2 - \Omega_1^2}\left(k_y^2 + \frac{k_y\delta\Omega_1}{\omega}\right) + \frac{\alpha_2\Omega_2}{\omega^2 - \Omega_2^2}\left(k_y^2 + \frac{k_y\delta\Omega_2}{\omega}\right) \\ &\quad = \frac{eB}{KT_e}\frac{\omega_* + ib\sigma_\parallel}{\omega + ib\sigma_\parallel} . \end{aligned} \quad \text{(A17)}$$

When the density gradient is small, the frequency shift $\Delta\omega$ created by the inhomogeneity can be approximated by

expanding Eq. (A17) about the homogeneous-plasma solution. For the two-ion hybrid root where $k_z^2/k_y^2 \ll 1$, $\alpha_2 \ll 1$, and $|\Delta\Omega| \ll \Omega_2$, we obtain

$$\mathrm{Re}(\Delta\omega) \simeq -\alpha_2(\omega_*/\omega_B)(\Delta\Omega/\Omega_2)(\Delta\Omega - \alpha_2\Omega_2) , \tag{A18}$$

$$\mathrm{Im}(\Delta\omega) \simeq -2\alpha_2(k_z^2/k_y^2)[(\Delta\Omega)^2/\Omega_2]\omega_c\tau_{ei} , \tag{A19}$$

where $\Delta\Omega \equiv \Omega_2 - \Omega_1$ and $\omega_B = k_y^2 D_B$ is the frequency for Bohm diffusion across a perpendicular wavelength. We see that $\Delta\omega$ is extremely small for the experiment in question because it depends not only on the density gradient but also on the fractional concentration of the minor species and on the mass difference between the ion species.

[1]S. J. Buchsbaum, Phys. Fluids **3**, 418 (1960).

[2]F. F. Chen, *Introduction to Plasma Physics and Controlled Fusion*, 2nd ed. (Plenum, New York, 1984), Vol. 1, Eqs. [4-80], [B-10], [7-118], [4-67], [7-11], and [7-15].

[3]T. H. Stix, *Theory of Plasma Waves* (McGraw-Hill, New York, 1962), pp. 10 and 89.

[4]B. D. Fried and S. Conte, *The Plasma Dispersion Function* (Academic, New York, 1961).

[5]R. W. Motley and N. D'Angelo, Phys. Fluids **6**, 296 (1963).

[6]G. Dimonte, T. Christensen, G. R. Neil, and T. E. Romesser, Bull. Amer. Phys. Soc. **24**, 992 (1979).

[7]R. W. Motley and T. Kawabe, Phys. Fluids **14**, 1019 (1971).

[8]R. K. Fisher and R. W. Gould, Phys. Fluids **14**, 857 (1971).

[9]F. F. Chen, Plasma Phys. **7**, 399 (1965).

[10]F. F. Chen. Phys. Fluids **22**, 2346 (1979).

[11]F. F. Chen, Phys. Fluids **7**, 949 (1964); **8**, 1323 (1965); and **9**, 965 (1966); H. W. Hendel and T. K. Chu, in *Methods of Experimental Physics*, edited by H. R. Griem and R. H. Lovberg (Academic, New York, 1970), Vol. 9, Part A, p. 345.

[12]B. B. Kadomtsev, *Plasma Turbulence* (Academic, New York, 1965), p. 84.